

Suppression of the Biermann Battery and Stabilization of the Thermomagnetic Instability in Laser Fusion Conditions

M. Sherlock^{1,*} and J. J. Bissell²

¹*Lawrence Livermore National Laboratory, P.O. Box 808, Livermore, California 94551, USA*

²*Department of Electronic Engineering, University of York, York YO10 5DD, United Kingdom*

 (Received 18 July 2019; accepted 15 January 2020; published 3 February 2020)

Magnetic field generated by the Biermann battery is thought to be one of the principal mechanisms behind the inhibition of heat flow in laser-plasma interactions, and is predicted to grow exponentially in some contexts due to the thermomagnetic instability [Tidman and Shanny, *Phys. Fluids* **17**, 1207 (1974)]. In contrast to these predictions, however, we have conducted Vlasov-Fokker-Planck simulations of magnetic field dynamics under a range of classically unstable laser-fusion conditions, and find field generation to be strongly suppressed, preventing magnetization of the transport, and stabilizing instability. By deriving new scaling laws, we show that this stabilization is a consequence of (i) heavy suppression of the Biermann battery under nonlocal conditions; (ii) rapid convection of magnetic field by the heat flow; and (iii) comparatively short field length scales. Our results indicate that classical models substantially overestimate the importance of magnetic fields generated by the Biermann battery, and the susceptibility of laser-fusion plasmas to the thermomagnetic instability.

DOI: [10.1103/PhysRevLett.124.055001](https://doi.org/10.1103/PhysRevLett.124.055001)

The generation of magnetic field during the interaction of high power lasers with plasmas is a topic of importance for both fundamental plasma physics and laser-fusion research, primarily because magnetic fields strongly affect transport of thermal energy [1]. Multimegagauss magnetic fields are readily generated in a variety of laboratory plasma experiments, including those relevant to inertial confinement fusion (ICF) [2–5]. The main source of magnetic field (flux density \mathbf{B}) in these cases is the Biermann battery (the *baroclinic* mechanism), which occurs when gradients in the electron number density n_e and temperature T_e are non-parallel, and at the rate $\partial\mathbf{B}/\partial t = \nabla T_e \times \nabla n_e / en_e$ (elementary charge e) [2,4]. Under conditions involving feedback from magnetized thermal transport (heat flow), the baroclinic mechanism is believed to generate filamentary magnetic field at an exponential rate by an effect known as thermomagnetic instability [6,7]. For example, the onset of thermomagnetic instability has been proposed as one of the main causes of filamentary structures in coronal plasmas, and as an explanation behind the need for thermal flux inhibition when interpreting laser-plasma experiments [8–11]. Despite these important applications, however, studies of the instability have been limited to classical linear models, unsupported by numerical simulation, meaning that the relevance of the thermomagnetic mechanism to nonlocal, laser-fusion conditions has remained largely untested [6,7,12–15]. It has long been known, for example, that classical transport models of laser-plasma coronas are invalid (because the plasma is typically so hot and rarefied that the electron mean-free-path λ_{ei} is large compared to

system scale lengths), and under these conditions kinetic simulations become essential [16,17].

In this Letter, therefore, we report the first kinetic study of the thermomagnetic instability, with a special focus on its consequences for magnetized transport in laser-fusion plasmas. Crucially, we present the first simulations of the thermomagnetic instability of any kind, and—contrary to classical theory—find it to be stabilized for conditions relevant to laser fusion. By deriving new scaling laws, we show that the principal mechanisms behind this stabilization are (i) reduced strength of the Biermann battery due to nonlocality; (ii) rapid convection of magnetic field with the heat flow (the Nernst effect); and (iii) the large electron mean-free-path compared to the size of field perturbations. Beyond the immediate context of laser fusion, however, the thermomagnetic instability provides an ideal test bed for quantifying the interplay between magnetic field generation, Nernst convection, and magnetized heat flow more generally [13]. Our scaling laws suggest that the mechanisms (i), (ii), and (iii) described above will severely limit the impact of magnetic fields generated by the Biermann battery in a wide variety of laser-plasma conditions.

The physical processes involved in the thermomagnetic instability are shown in Fig. 1, assuming a geometry in which the plasma is taken to have bulk zeroth-order electron number density $n_0(x)$, and temperature $T_0(x)$ gradients in the x direction only. Should a first-order transverse temperature perturbation $\delta T(y)$ arise (due, e.g., to variation in laser intensity), then a Biermann magnetic field perturbation $\delta B_z(y) \propto |\nabla\delta T \times \nabla n_0|$ is generated in the z direction; this in turn induces a y -directed

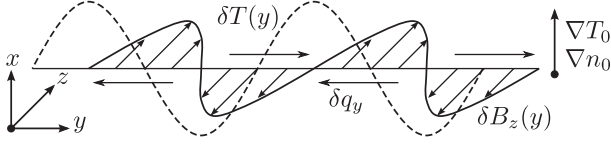


FIG. 1. Thermomagnetic instability mechanism [6,7] depicting the bulk density and temperature gradients ∇n_0 and ∇T_0 , the temperature perturbation $\delta T(y)$ (dashed curve), the induced field $\delta B_z(y)$ (solid curve with arrows), and the resulting Righi-Leduc heat flow δq_y (arrows in the y direction).

Righi-Leduc heat flow δq_y , toward the hotter regions of the temperature perturbation [1,6,7], driving positive feedback, and unstable growth of Biermann filaments.

Growth rates γ can be derived from a linear perturbation analysis of the classical transport equations [1] assuming $\delta T, \delta B_z \propto \exp(\gamma t + iky)$, with wave number k [12–14]. In this way one obtains the dispersion relation

$$\gamma_{\pm} = \frac{1}{2} \left\{ -[(d_T + d_R)k^2 - \tilde{N}] \pm \sqrt{[(d_T + d_R)k^2 - \tilde{N}]^2 + 4d_T k^2 [d_R(k_G^2 - k^2) + \tilde{N}]} \right\}, \quad (1)$$

where instability prevails whenever $\gamma_{\pm} > 0$, and terms describe the following: thermal diffusion d_T ; resistive diffusion d_R ; magnetic-field generation by the Biermann battery (coupled to Righi-Leduc) k_G^2 ; and advection of the magnetic field by the Nernst effect \tilde{N} . These terms are defined by

$$d_T = \frac{c_B \kappa_{\perp} \lambda_{ei}^2}{3 \tau_{ei}}, \quad k_G^2 = \frac{c_B^2}{2\alpha_{\perp} \kappa_{\perp} \delta^2} \frac{\partial \kappa_{\perp}}{\partial \chi} \frac{\lambda_{ei}^2}{l_T l_n}, \quad (2)$$

$$d_R = \frac{\alpha_{\perp} \lambda_{ei}^2}{c_B \Lambda^2 \tau_{ei}}, \quad \tilde{N} = \frac{c_B}{2} \frac{\partial \beta_{\perp}}{\partial \chi} \frac{\lambda_{ei}^2}{\tau_{ei}^2 T_0} \frac{\partial}{\partial x} \left[\tau_{ei} \frac{\partial T_0}{\partial x} \right], \quad (3)$$

where $l_T \equiv T_0/(\partial T_0/\partial x)$ and $l_n \equiv n_0/(\partial n_0/\partial x)$ are the bulk temperature and density length scales, respectively, and the remaining parameters are the following: the electron mass m_e ; the ratio $\Lambda \equiv \lambda_{ei}/\delta$, with skin depth $\delta = \sqrt{m_e/\mu_0 n_e e^2}$, where μ_0 is the permeability of free space; the Braginskii collision time $\tau_B = c_B \tau_{ei}$, with $c_B = 3\sqrt{\pi}/4$ a dimensionless constant; and the electron-ion thermal collision time $\tau_{ei} = (4\pi v_T^3)/(n_i [Ze^2/\epsilon_0 m_e]^2 \log \Lambda_{ei})$, where $\log \Lambda_{ei}$ is the Coulomb logarithm, $v_T = \lambda_{ei}/\tau_{ei} = (2T_e/m_e)^{1/2}$ the thermal velocity, ϵ_0 the permittivity of free space, Z the atomic number, and $n_i \approx n_e/Z$ the ion number density [12]. The transport coefficients—the resistive diffusivity α_{\perp} , the thermal diffusivity κ_{\perp} , the Righi-Leduc coefficient κ_{\perp} , and the Nernst coefficient β_{\perp} —are dimensionless functions of Z , and the Hall parameter $\chi \equiv \omega_L \tau_B$, with $\omega_L = e|\mathbf{B}|/m_e$; these coefficients are expected to be strongly affected by nonlocal conditions [13,16,17].

Crucially for our study, the analysis used to derive Eq. (1) makes assumptions which will not hold rigorously in practical contexts [12]. For example, the Biermann term scales as $k_G^2 \propto \lambda_{ei}^2/l_n l_T$, while the Nernst term scales as $\tilde{N} \tau_{ei} \propto \lambda_{ei}^2 (\partial/\partial x) [\tau_{ei} (\partial T_0/\partial x)] / \tau_{ei} T_0 \sim \lambda_{ei}^2/l_T^2$, meaning that growth rates are largest when length scales $l_{n,T}$ are short compared to the mean-free-path λ_{ei} , i.e., precisely those contexts where nonlocality is important. Nevertheless, the dispersion relation does provide a useful means for estimating the impact of effects.

Ignoring for the moment the Nernst term \tilde{N} , plasma conditions representative of an ICF hohlraum corona ($T_e \approx 3$ keV, $Z \approx 50$, $n_e \approx 10^{27} \text{ m}^{-3}$, $l_n \approx 100 \mu\text{m}$, and $l_T \approx 30 \mu\text{m}$) suggest a peak growth rate of $\gamma \approx 10^{12} \text{ s}^{-1}$ at wavelength $\lambda = 2\pi/k \approx 17 \mu\text{m}$, so that the instability can be expected to develop within typical nanosecond pulse lengths, and generate small filaments. Some authors have argued that Nernst advection is likely to increase the growth rate further [14,17], while others propose that fluid motion alone will reduce the growth rate if it becomes comparable to hydrodynamic rates [15]. However, in the region close to critical, where the heat flux is greatest, we find that the Nernst effect is the dominant convective process; this is because typical Nernst velocities $\mathbf{v}_N \approx -(2/5)\kappa_{\perp} \nabla T_e / (n_e T_e) \sim 10^6 \text{ ms}^{-1}$ (inward) [10,13] in the plasma corona greatly exceed the typical ablation velocity $\mathbf{v}_A \sim 10^5 \text{ ms}^{-1}$ (outward).

For our numerical study of the instability we use the kinetic code K2 [18,19] which solves the Vlasov-Fokker-Planck equation by expanding the electron distribution function f in spherical harmonics (here truncated before second-order to prevent collisional Weibel modes from complicating the analysis [20]). We include electron-electron collisions on f_0 and account for electron-electron collisions on f_1 by multiplying the electron-ion scattering frequency by the factor $(Z + 0.24)/(Z + 4.2)$, which is close to unity for our conditions. This common approximation is discussed in more detail in, e.g., [21,22]. From [22] we estimate that the error associated with this approximation for the case of carbon ($Z^* = 6$) and helium ($Z^* = 2$) are about 28% and 220%, respectively. Our results are therefore only qualitative in the case of low- Z gases. Maxwell's equations are solved implicitly, which is necessary to avoid artificial \mathbf{B} -field generation in problems involving large heat fluxes. Bulk fusion conditions corresponding to a dense target on the left boundary with a linear rise in the coronal region on the right are modeled by setting the electron density to $n_e = H(x, l_x) + 6[(x - 0.15l_x)/l_c] \times 10^{27} \text{ m}^{-3}$, where l_c is the coronal length scale, l_x is the x -domain size, and $H(x, l_x) = \tilde{n}_0 + (\tilde{n}_1 - \tilde{n}_0) \{1 + \tanh[(x - 0.15l_x)/0.1l_x]\}/2$, with densities $\tilde{n}_0 = 5 \times 10^{28} \text{ m}^{-3}$, and $\tilde{n}_1 = 2 \times 10^{26} \text{ m}^{-3}$. We select $Z^* = 50$ to represent an underdense Au target. These conditions were motivated by radiation hydrodynamics simulations of hohlraums of the type shown in, e.g., [23],

in which significant volumes of the underdense plasma region satisfy the criteria for instability.

Heating of the plasma in the underdense region ($n_e < 9.1 \times 10^{27} \text{ m}^{-3}$) is modeled according to the rate $\partial T_e / \partial t = [\tilde{T}(x; l_x, l_y) \times 2.7 \text{ keV} - T_e] / \text{ps}$, where $\tilde{T}(x) = (1 - \varepsilon \cos[2\pi y / l_y]) \{1 + \tanh[(x - 0.7l_x) / 0.2l_x]\} / 2$, with $\varepsilon = 0.02$, and y -domain size l_y . This induces a transversely perturbed heat flow toward the dense target with wavelength l_y . The left-hand boundary is maintained close to a temperature of 1 keV to approximate the effect of radiative cooling of the target. The strength of the perturbation is influenced by the parameter ε , but determined self-consistently by thermal transport. Increasing ε does not change our main conclusions. Notice that the domain size can be varied to study a range of perturbation wavelengths, and plasma scale lengths (though we fix the coronal scale at $l_c = 100 \mu\text{m}$), with boundary conditions reflective in x , and periodic in y .

A set of profiles from a typical simulation is shown in Fig. 2; only the corona satisfies the $k_G^2 > 0$ condition for field generating instability (due to the sign of $l_T l_n$), and for this reason we direct our attention to this region (e.g., $x \gtrsim 20 \mu\text{m}$ for $l_x = 100 \mu\text{m}$). Here, we focus on four simulations by setting $(l_x, l_y) = (n_s \times 25 \mu\text{m}, l_x / 2)$, with $n_s \in \{1, 2, 3, 4\}$; this allows us to examine four degrees of nonlocality relevant to ICF plasmas, with peak values of λ_{ei} / l_T ranging from 0.009 to 0.22. Each simulation is run for $t \gtrsim 10^2$ ps (i.e., ~ 50 classical growth periods).

As seen by the Hall parameter $\chi = \omega_L \tau_B$ data in Fig. 2(b) (data for the $l_x = 100 \mu\text{m}$ case, with $\lambda_{ei} / l_T \approx 0.027$), the coronal region is more magnetized than the target surface because of the longer collision time τ_{ei} . However, the peak

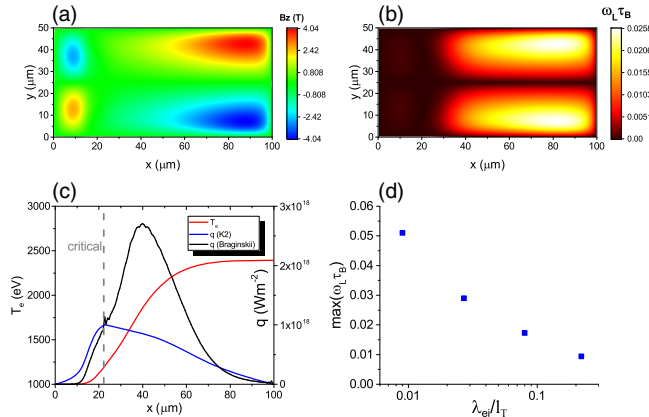


FIG. 2. The \mathbf{B} field (a) and Hall parameter (b) for the $l_x = 100 \mu\text{m}$ ($n_s = 4$) case at 360 ps. Plot (c) displays lineouts ($y = 37 \mu\text{m}$) of the temperature T_e and heat flux $q = |q_x|$ for the $l_x = 100 \mu\text{m}$ case at 20 ps, where the dashed line is the critical surface (the classical Braginskii heat flux q_B is displayed for comparison). Plot (d) shows the maximum Hall parameter that develops in the corona for each simulation n_s , plotted against the corresponding nonlocality parameter.

Hall parameter remains small ($\chi \approx 0.026$), indicating that the magnetic field fails to grow to levels capable of affecting transport, or inducing thermomagnetic instability; this contrasts with the classically predicted e -folding time $t_\gamma = \gamma^{-1}$ for these conditions of 5–20 ps, which is well within the simulation run time (700 ps).

Nonlocal suppression of the heat flux q_x into the target (for the $l_x = 100 \mu\text{m}$ case) is shown in the lineouts displayed in Fig. 2(c). In each simulation, the peak magnetic field in the corona rises approximately linearly with time (rather than unstable, exponential growth), and saturates after ~ 500 ps. The peak values of the Hall parameter during the simulation are shown in Fig. 2(d), and plotted against the corresponding (peak) nonlocality parameter λ_{ei} / l_T , indicating it is more difficult to magnetize the corona as the nonlocality increases. In all cases, the Hall parameter is minimal ($\chi \ll 1$).

We now explore the reasons for the lack of magnetization of the corona by considering \mathbf{B} -field evolution according to the induction equation. Under classical conditions the induction equation is dominated by the Biermann and Nernst terms, i.e.,

$$\frac{\partial \mathbf{B}}{\partial t} = \frac{\nabla T_e \times \nabla n_e}{en_e} + \nabla \times (\mathbf{v}_N \times \mathbf{B}), \quad (4)$$

where $\mathbf{v}_N \approx (-2\kappa_\perp \nabla T_e / 5n_e T_e)$ is the Nernst velocity [10]. In nonlocal conditions, however, this equation takes the more general form [16,24]

$$\frac{\partial \mathbf{B}}{\partial t} = \frac{m_e \nabla(n_e \langle v^5 \rangle) \times \nabla(n_e \langle v^3 \rangle)}{6en_e^2 \langle v^3 \rangle^2} + \nabla \times (\tilde{\mathbf{v}}_N \times \mathbf{B}), \quad (5)$$

where the angle brackets $\langle v^m \rangle \equiv (4\pi/n_e) \int_0^\infty f_0 v^{m+2} dv$ denote velocity v moments over the isotropic component of the distribution $f_0(v)$, with $m \in \mathbb{Z}$. Note that the first term above describes generalized baroclinic field generation (accounting for deviations from the classical Biermann rate), while $\tilde{\mathbf{v}}_N = \langle \mathbf{v} v^3 \rangle / 2 \langle v^3 \rangle$ is the generalized Nernst velocity; both expressions reduce to their classical forms when f_0 is Maxwellian, i.e., $f_0 \propto e^{-v^2}$.

Comparing Eqs. (4) and (5), the magnetic field fails to grow under nonlocal conditions for two main reasons: first, the generalized baroclinic field generation rate is much lower compared to the classical (Biermann) rate; and second, the generalized Nernst effect $\tilde{\mathbf{v}}_N$ remains strong enough to advect the field out of the generation zone. Both effects are quantified in Figs. 3(a) and 3(b), where we plot the peak values of the two terms in Eq. (5) normalized to their classical values of Eq. (4); this gives us a measure of how much the induction terms deviate from classical expectations as a function of nonlocality λ_{ei} / l_T , with both processes suppressed as nonlocality increases. Note that in each case we focus on peak values at the location $(x, y) = (0.9l_x, 0.75l_y)$, which is always near the region

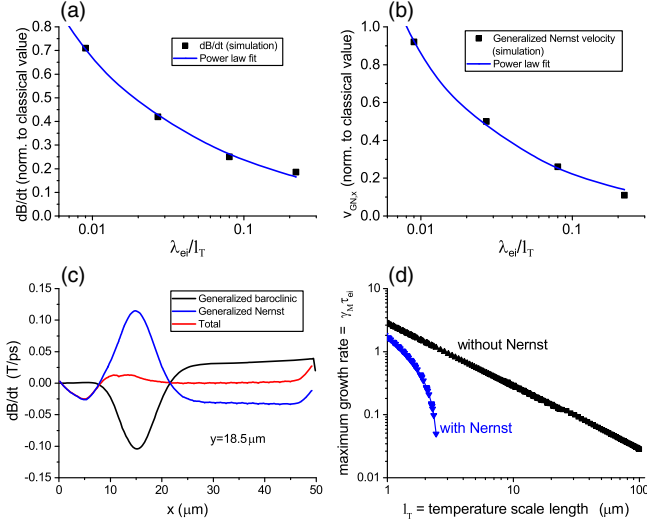


FIG. 3. (a) The generalized baroclinic field generation rate, and (b) the generalized Nernst velocity, each normalized to their classical value, as a function of nonlocality. (c) Lineouts (at $y = 18.5 \mu\text{m}$) of the generalized baroclinic and Nernst convection rates at 180 ps for the $l_x = 50 \mu\text{m}$ simulations, showing the approximate cancellation of the two terms throughout the corona (the total field generation rate is plotted for comparison). (d) The peak instability growth rate γ_M of Eq. (1) as a function of the thermal scale length l_T , for typical ICF conditions (with and without the Nernst term).

of peak coronal magnetic field; however, comparable levels of deviation from classical predictions are found throughout the simulation. Power law fits to the simulation data give a convenient means of determining the approximate degree of reduction for a given nonlocality, in particular, we find that the nonlocal baroclinic and Nernst terms follow

$$\frac{\partial B}{\partial t} \approx 0.083 \left(\frac{\lambda_{ei}}{l_T} \right)^{-0.453} \left(\frac{\partial B}{\partial t} \right)_{\text{classical}}, \quad (6)$$

$$\text{and } |\tilde{\mathbf{v}}_N| = \tilde{v}_N \approx 0.0566 \left(\frac{\lambda_{ei}}{l_T} \right)^{-0.593} v_N, \quad (7)$$

where $(\partial B/\partial t)_{\text{classical}} = |\nabla n_e \times \nabla T_e|/en_e$ is the magnitude of the classical Biermann battery, and $v_N = |\mathbf{v}_N|$ is the magnitude of the classical Nernst velocity. These fits are valid in the interval $\lambda_{ei}/l_T = [0.009, 0.22]$, and should be prevented from exceeding unity if used at lower λ_{ei}/l_T . We add that—in addition to the hohlraum coronal plasma conditions considered here—we have performed complementary simulations using conditions relevant to direct-drive plasmas, which also closely follow power laws (6) and (7).

Although the Nernst velocity is reduced under nonlocal conditions, the Nernst effect nevertheless impairs magnetization because it advects the magnetic field from the corona where it is generated, and into the dense target region (i.e., in the direction of the heat flow). To illustrate this, consider the lineout (at $y = 18.5 \mu\text{m}$) of the x -directed heat flow (the

dominant heat-flow direction) shown in Fig. 3(c); this figure indicates that the rate of field generation by the baroclinic mechanism is approximately balanced by the rate of Nernst convection of the field into the target, significantly reducing the total rate of change of coronal magnetic field. The stabilizing effect of Nernst convection was previously demonstrated in kinetic studies of the collisional Weibel instability [25].

Note that although the Righi-Leduc heat flow plays a key role in the field-generating instability, we find that it is negligible in our simulations due to both the lack of magnetization, and the effect of what might be termed *magnetic nonlocality*: the ability of the heat-carrying electrons to escape the region of magnetic field. Although nonlocality is usually defined with respect to temperature scale lengths by λ_{ei}/l_T , when a magnetic field is present transport is also characterized by a magnetic nonlocality parameter $M \equiv r_L/l_B$, where $r_L = v_T/\omega_L$ is the Larmor radius, with $l_B = |B_z|/\max(\partial B_z/\partial x, \partial B_z/\partial y)|$ as the shortest scale length of the magnetic field perpendicular to its direction. Thus, for the heat-carrying electrons (velocity $\approx 2.6v_T$) to complete a Larmor orbit without leaving the field region, we require $2.6r_L < l_B$ or $M \equiv r_L/l_B \lesssim 0.38$ (in addition to the usual condition $\chi \gtrsim 1$). The Hall parameter does not account for variations in the magnetic field strength experienced by the electron during the period of collisional or magnetic confinement. This concept also applies to the other transport effects involving magnetization of energetic electrons, for example, the cross-field heat flow \mathbf{q}_\perp . Since our simulations are in the range $0.5 \lesssim M \lesssim 42$, we expect magnetic nonlocality to be a key further reason for the lack of magnetization: heat-carrying electrons leave the magnetic field region before significant deflection, limiting its effect.

It is interesting to note that the classically derived expression for the thermomagnetic instability growth rate γ_+ of Eq. (1) is consistent with the stabilization seen in our simulations, even though the classical model is expected to break down for nonlocal conditions. Although our simulations show that nonlocal effects are important, the inclusion of the classical Nernst convection term is itself enough to predict stabilization, with $\tilde{N} = (c_B/2) \times (\partial \beta_\perp/\partial \chi)(\lambda_{ei}^2/\tau_{ei}^2 T_0)(\partial/\partial x)[\tau_{ei}\partial T_0/\partial x]$ undetermined by the perturbation analysis, and therefore appearing as a function of the bulk plasma conditions. Most previous studies [6,14,15] neglected \tilde{N} , or only considered the case in which \tilde{N} is positive, which leads to an enhancement of the growth rate, as motivated by the idea that Nernst convection can compress the magnetic field [26]. Nevertheless, Bol'shov [8] and Haines [27] have pointed out that the thermoelectric effects could lead to saturation of the field, which is the expected behavior when $\tilde{N} < 0$, with Nernst convection rarefying the field.

The behavior of \tilde{N} can be investigated by modeling the bulk temperature T_0 according to a “quasi-Gaussian”

profile of the form $T_0(x) = \hat{T}_0(1 + \sin[2\pi x/\hat{l}_T])$, where \hat{l}_T is the scale length of T_0 , with \hat{T}_0 as the half maximum. Under these assumptions $\tilde{N}(x)$ takes its greatest value at $x = \hat{l}_T/4$, with

$$\tilde{N}(\hat{l}_T/4) = -3072 \left(\frac{\partial \beta_\wedge^c}{\partial \chi} \right) \frac{\epsilon_0^4 \pi^{9/2} \hat{T}_0^4}{\tau_{ei} (Ze^4 n_e \log \Lambda_{ei})^2}, \quad (8)$$

where the thermoelectric derivative $\partial \beta_\wedge^c / \partial \chi$ is calculated from the polynomial fits [28]. The inclusion of this term in the dispersion relation of Eq. (1) is sufficient to reduce the growth rate below zero for parameters typical of laser-plasma coronas. As an example, the growth rate is plotted in Fig. 3(d) as a function of the background temperature scale length for the conditions $T_0 = 3$ keV, $n_e = 10^{27} \text{ m}^{-3}$, $Z = 50$, $\hat{l}_T = l_y$, and $\tilde{N} = \tilde{N}(\hat{l}_T/4)/2$; this represents a conservative estimate for the effect of Nernst damping, because in realistic scenarios the background temperature scale length \tilde{l}_T is shorter than the transverse perturbation scale length l_y , and therefore Nernst convection is more rapid. The efficient damping by Nernst across a wide range of ICF-relevant temperature scale lengths, indicated in Fig. 3(d), supports the conclusion drawn from the kinetic simulations.

We note a promising platform for the study of magnetized transport instabilities could involve the heating of a uniform gas by radiation from a pulsed-power device. By using a gauze, the wavelength of the heat source could be varied and magnetic field strength measured as a function of this wavelength and gas density [29].

In summary, we have performed 2D Vlasov-Fokker-Planck simulations of magnetic field generation by the Biermann battery (and, more generally, the baroclinic mechanism) in laser-plasma interactions relevant to inertial fusion, including the first numerical study of field generation by the thermomagnetic instability [6,7]. Contrary to classical expectation, we find that the ability of self-generated magnetic fields to affect transport is strongly inhibited by three key mechanisms: (i) a reduction of the baroclinic (Biermann) rate of field generation in nonlocal conditions; (ii) the convection of fields out of the generation region by the generalized Nernst effect; and (iii) the relatively small size of magnetic field regions compared to the Larmor radius of the heat-carrying electrons (“magnetic nonlocality”). Crucially, these mechanisms stabilize the thermomagnetic instability in conditions relevant to laser fusion, and significantly reduce the effect of magnetic fields on transport in coronal plasmas.

This work was performed under the auspices of the U.S. Department of Energy by LLNL under Contract No. DE-AC52-07NA27344 and release No. LLNL-JRNL-730526.

*Corresponding author.

sherlock3@llnl.gov

- [1] S. I. Braginskii, in *Reviews of Plasma Physics*, edited by M. A. Leontovich (Consultants Bureau, New York, 1965), Vol. 1, p. 205.
- [2] J. A. Stamper and B. H. Ripin, *Phys. Rev. Lett.* **34**, 138 (1975).
- [3] P. M. Nilson *et al.*, *Phys. Rev. Lett.* **97**, 255001 (2006).
- [4] C. Li *et al.*, *Phys. Rev. Lett.* **102**, 205001 (2009).
- [5] A. Raven, O. Willi, and P. T. Rumsby, *Phys. Rev. Lett.* **41**, 554 (1978).
- [6] D. A. Tidman and R. A. Shanny, *Phys. Fluids* **17**, 1207 (1974).
- [7] L. A. Bol’shov, Yu. A. Dreizin, and A. M. Dykhne, *JETP Lett.* **19**, 168 (1974).
- [8] L. A. Bol’shov, Yu. A. Dreizin, A. M. Dykhne, V. P. Kiselev, A. P. Favorskii, and A. I. Yudin, *Sov. Phys. JETP* **50**, 1101 (1979).
- [9] O. Willi and P. T. Rumsby, *Opt. Commun.* **37**, 45 (1981).
- [10] M. G. Haines, *Can. J. Phys.* **64**, 912 (1986).
- [11] M. J.-E. Manuel *et al.*, *Phys. Plasmas* **20**, 056301 (2013).
- [12] J. J. Bissell, *J. Plasma Phys.* **81**, 905810108 (2015).
- [13] J. J. Bissell, C. P. Ridgers, and R. J. Kingham, *New J. Phys.* **15**, 025017 (2013).
- [14] A. Hirao and M. Ogasawara, *J. Phys. Soc. Jpn.* **50**, 668 (1981).
- [15] M. Ogasawara, A. Hirao, and H. Ohkubo, *J. Phys. Soc. Jpn.* **49**, 322 (1980).
- [16] R. J. Kingham and A. R. Bell, *Phys. Rev. Lett.* **88**, 045004 (2002).
- [17] A. R. Bell, R. G. Evans, and D. J. Nicholas, *Phys. Rev. Lett.* **46**, p243 (1981).
- [18] M. Sherlock, J. P. Brodrick, and C. P. Ridgers, *Phys. Plasmas* **24**, 082706 (2017).
- [19] A. R. Bell, A. P. L. Robinson, M. Sherlock, R. J. Kingham, and W. Rozmus, *Plasma Phys. Controlled Fusion* **48**, R37 (2006).
- [20] E. S. Weibel, *Phys. Rev. Lett.* **2**, 83 (1959).
- [21] J. P. Brodrick, R. J. Kingham, M. M. Marinak, M. V. Patel, A. V. Chankin, J. T. Omotani, M. V. Umansky, D. Del Sorbo, B. Dudson, J. T. Parker, G. D. Kerbel, M. Sherlock, and C. P. Ridgers, *Phys. Plasmas* **24**, 092309 (2017).
- [22] J. P. Brodrick, M. Sherlock, W. A. Farmer, A. S. Joglekar, R. Barrios, J. Wengraf, J. J. Bissell, R. J. Kingham, D. Del Sorbo, M. P. Read, and C. P. Ridgers, *Plasma Phys. Controlled Fusion* **60**, 084009 (2018).
- [23] O. S. Jones, L. J. Suter, H. A. Scott, M. A. Barrios, W. A. Farmer, S. B. Hansen, D. A. Liedahl, C. W. Mauche, A. S. Moore, M. D. Rosen, J. D. Salmonson, D. J. Strozzi, C. A. Thomas, and D. P. Turnbull, *Phys. Plasmas* **24**, 056312 (2017).
- [24] M. G. Haines, *Plasma Phys. Control. Fusion* **28**, 1705 (1986).
- [25] E. M. Epperlein and A. R. Bell, *Plasma Phys. Control. Fusion* **29**, 85 (1987).
- [26] A. Nishiguchi, T. Yabe, M. G. Haines, M. Psimopoulos, and H. Takewaki, *Phys. Rev. Lett.* **53**, 262 (1984).
- [27] M. G. Haines, *Phys. Rev. Lett.* **78**, 254 (1997).
- [28] E. M. Epperlein and M. G. Haines, *Phys. Fluids* **29**, 1029 (1986).
- [29] S. V. Lebedev (private communication).